

Equivariant Sampling for Improving Diffusion Model-based Image Restoration

Chenxu Wu^{1,2} Qingpeng Kong^{1,2} Peiang Zhao^{1,2} Wendi Yang^{1,2}
 Wenxin Ma^{1,2} Fenghe Tang^{1,2} Zihang Jiang^{1,2*} S. Kevin Zhou^{1,2,3,4*}

¹ School of Biomedical Engineering, Division of Life Sciences and Medicine, USTC

² MIRACLE Center, Suzhou Institute for Advance Research, USTC

³ Key Laboratory of Intelligent Information Processing of CAS, ICT, CAS

⁴ State Key Laboratory of Precision and Intelligent Chemistry, USTC

wuchexu@mail.ustc.edu.cn jzh0103@ustc.edu.cn s.kevin.zhou@gmail.com

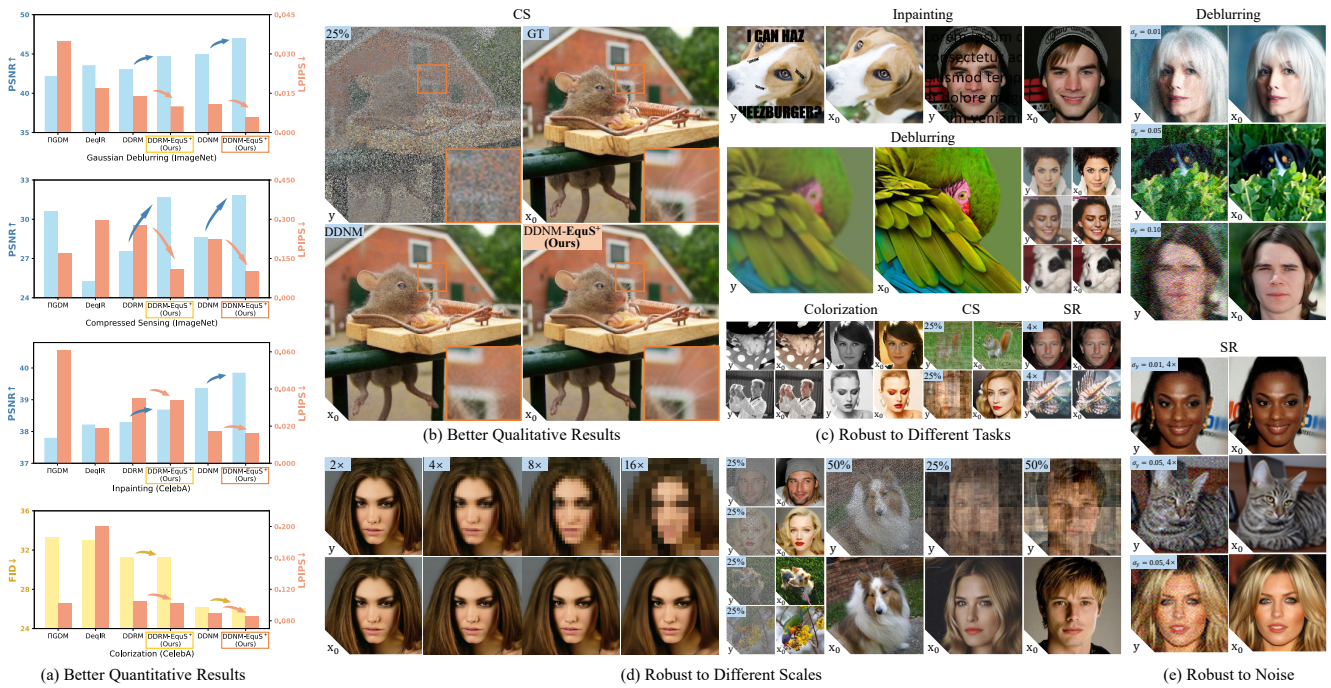


Figure 1. Our method offers (a) superior quantitative performance, (b) improved qualitative results. It is (c) adaptable to various IR applications, (d) robust to different scales, and (e) resilient to different noise levels. y represents the degraded image, x_0 denotes the sampling result, SR represents super-resolution and CS represents compressed-sensing.

Abstract

Recent advances in generative models, especially diffusion models, have significantly improved image restoration (IR) performance. However, existing problem-agnostic diffusion model-based image restoration (DMIR) methods face challenges in fully leveraging diffusion priors, resulting in sub-optimal performance. In this paper, we address the limitations of current problem-agnostic DMIR methods by analyzing their sampling process and providing effective solutions. We introduce *EquS*, a DMIR method that imposes equivariant information through dual sampling trajectories. To further boost *EquS*, we propose the *Timestep-*

Aware Schedule (TAS) and introduce *EquS*⁺. *TAS* prioritizes deterministic steps to enhance certainty and sampling efficiency. Extensive experiments on benchmarks demonstrate that our method is compatible with previous problem-agnostic DMIR methods and significantly boosts their performance without increasing computational costs. Our code is available in the Supplementary.

1. Introduction

Image restoration (IR) aims to recover the original image from a degraded image. It remains a longstanding challenge due to its ill-posed nature and significant practical ap-

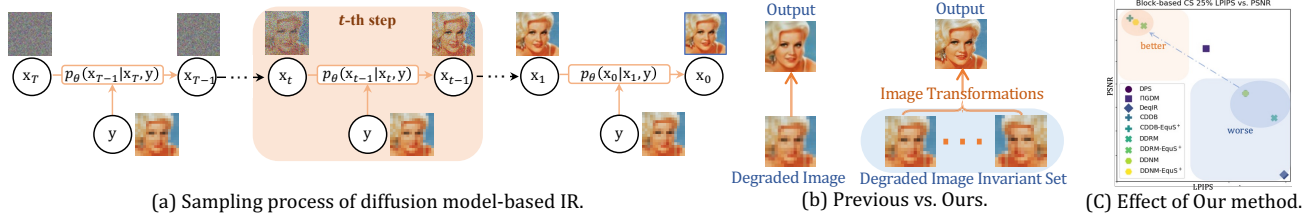


Figure 2. (a) Sampling process of diffusion model-based IR. (b) Previous vs. Ours. (c) Effect of our methods.

plications [3, 69]. Traditional IR methods [9–11, 28, 29, 32, 55, 101] are limited to single-task solutions, requiring multiple deep neural network (DNN) trainings. Recently, diffusion models [39, 75, 78, 79] have emerged as powerful generative models [27, 70], offering a fresh approach to IR. Their ability to model complex, high-dimensional distributions positions them as effective solutions for addressing problem-specific IR challenges [25], encompassing applications such as super-resolution [19, 34, 52, 73], deblurring [18, 68], inpainting [24, 60, 62], colorization [13, 90], and compressed sensing [22, 96].

Notably, a growing family of research [2, 12, 21, 31, 35, 44, 49, 88, 107] leverages diffusion models to address various IR tasks in a zero-shot manner. These problem-agnostic diffusion model-based image restoration (DMIR) methods can utilize diffusion priors from pre-trained diffusion models irrespective of the specific problem at hand. They achieve this by incorporating the degraded image via inverse guidance or conditioning during the sampling process, as shown in Figure 2 (a). However, these methods face challenges in fully leveraging diffusion priors, leading to suboptimal results.

First, these methods guide the sampling process based on unidirectional information, using a single sampling trajectory. The reliance on a single degraded image for determining the restoration output, as illustrated in Figure 2 (b), may hinder performance by introducing biases into the reconstructed image. Furthermore, when the degraded image is noisy, the stochasticity in the noise can exacerbate errors within a single sampling trajectory. Even minor errors may propagate through the long sampling chain inherent to diffusion models, leading to artifacts and reduced image quality. **Second**, previous methods implement a uniform sampling schedule, assigning equal importance to all time steps in the sampling process. However, in the context of DMIR, the degraded image is already close to the original image. Consequently, using a uniform schedule is suboptimal, as it concentrates too much on early steps that contribute little to the reconstruction. For instance, in tasks like super-resolution or deblurring, later steps often play a more critical role in refining details. Thus, employing a uniform schedule leads to inefficiencies and may reduce the accuracy of the final

reconstruction.

In this paper, we delve into the sampling process of DMIR, introducing **Equivariant Sampling (EquS)**—a DMIR method developed to fully leverage diffusion priors. Specifically, we incorporate an equivariant inverse mapping into the sampling process, introducing a novel approach that enables dual-trajectory sampling. By reinterpreting degraded images from an alternative perspective and facilitating their interaction with diffusion priors, EquS harnesses equivariant information to enhance reconstruction performance. To overcome the limitations of conventional uniform schedules in previous arts, we further propose the **Timestep-Aware Schedule (TAS)** and introduce an enhanced version of EquS, termed as **EquS⁺**. Unlike uniform schedules, TAS prioritizes deterministic time steps, introducing more certain information into the sampling outcomes and reducing sampling randomness, which is beneficial in IR where diversity in sampling outcomes is less critical. We conduct comprehensive experiments, demonstrating the exceptional performance of EquS and EquS⁺ across various IR tasks.

2. Related Work

IR frameworks. Researchers have explored frameworks that combine techniques such as residual blocks [45, 102, 106], attention mechanisms [8–11, 17, 53, 54, 94, 98, 100], GANs [6, 7, 36, 37, 63, 65–67, 84, 85, 103], and other methodologies [32, 41, 47, 55, 101] to enhance IR performance. Self-supervised learning approaches, such as Noise2X [4, 46, 48, 50, 61, 64, 82, 95] and equivariant imaging (EI) [14–16, 80], have also been explored as powerful frameworks for tackling IR challenges.

Problem-specific DMIR focuses on training conditional diffusion models either in the image space [30, 51, 57–59, 72, 73, 91, 92, 97, 99, 105] or in the latent space [56, 71, 83, 93]. In order to do this within a zero-shot framework, several methods utilize the diffusion priors, integrating the reference image during the sampling process [19, 60]. Overall, these methods predominantly concentrate on an individual IR task.

Problem-agnostic DMIR utilizes the diffusion priors of pre-trained models (DDPM [39], DDIM [76]) as versa-

tile, plug-and-play building blocks for solving various IR tasks. In the design of various guidance methods, DDRM [44] utilizes singular value decomposition (SVD) to the degradation operator, thereby tackling linear IR problems in a manner akin to SNIPS [43]. DDNM [88] computes the pseudo-inverse matrix for range-null space decomposition [74, 86], iteratively refining the null space in the sampling process. These advancements [20, 33, 87] further expand the applicability of DDNM. DeqIR [12] uses the guidance method in DDNM and presents a fixed-point solver for parallel sampling. DDPG [35] offers a guidance method that demonstrates robustness to noise. To further improve the IR performance, many methods consider computing deeper gradients for the guidance. For example, DPS [21] employs a Jensen approximation for posterior sampling. ZAPS [2] presents an alternative guidance methodology for DPS. IIGDM [77] introduces Jacobian calculation to pseudo-inverse guidance. CDDB [23] integrates the guidance method into I²SB [57], thereby enhancing its IR performance. However, all of these methods rely on a single sampling trajectory that considers only unidirectional information, which may lead to suboptimal performance.

3. Preliminaries

Problem Statement. IR focuses on restoring a high-quality image $\hat{\mathbf{x}}$ from a degraded image $\mathbf{y} = \mathbf{A}\mathbf{x} + \mathbf{n}$, where $\mathbf{y} \in \mathbb{R}^m$ represents the observed measurement, $\mathbf{x} \in \mathbb{R}^n$ denotes the original image, \mathbf{n} represents additive nonlinear noise (e.g., $\mathcal{N}(\mathbf{0}, \sigma_{\mathbf{y}}^2 \mathbf{I})$), and $\mathbf{A} \in \mathbb{R}^{m \times n}$ is a known measurement operator with $m \leq n$, e.g., a bicubic downsampler. The restoration process can be formulated as

$$\hat{\mathbf{x}} = \arg \min_{\mathbf{x}} \frac{1}{2\sigma^2} \|\mathbf{A}\mathbf{x} - \mathbf{y}\|_2^2 + \lambda \mathcal{R}(\mathbf{x}), \quad \lambda, \sigma \in \mathbb{R}, \quad (1)$$

where the first term, $\|\mathbf{A}\mathbf{x} - \mathbf{y}\|_2^2$, ensures data consistency, while the second term, $\lambda \mathcal{R}(\mathbf{x})$, introduces regularization based on prior knowledge of natural image, such as Tikhonov regularization [1].

Diffusion Models. DDPM [39] could generate high-quality images through a forward process and a reverse process. In the forward process, noise with specified levels is introduced to the data, *i.e.*,

$$q(\mathbf{x}_t | \mathbf{x}_0) := \mathcal{N}(\mathbf{x}_t; \sqrt{\bar{\alpha}_t} \mathbf{x}_0, (1 - \bar{\alpha}_t) \mathbf{I}), \quad (2)$$

where $\bar{\alpha}_t := \prod_{s=1}^t \alpha_s$, $\alpha_t := 1 - \beta_t$ and β_t is a variance of noise level. For the reverse process, the previous state \mathbf{x}_{t-1} can be predicted with $\tilde{\boldsymbol{\mu}}_t$ and $\tilde{\sigma}_t$, which is formulated as

$$q(\mathbf{x}_{t-1} | \mathbf{x}_t, \mathbf{x}_0) := \mathcal{N}(\mathbf{x}_{t-1}; \tilde{\boldsymbol{\mu}}_t(\mathbf{x}_t, \mathbf{x}_0), \sigma_t^2 \mathbf{I}), \quad (3)$$

where $\tilde{\boldsymbol{\mu}}_t(\mathbf{x}_t, \mathbf{x}_0) := \frac{\sqrt{\bar{\alpha}_{t-1}} \beta_t}{1 - \bar{\alpha}_t} \mathbf{x}_0 + \frac{\sqrt{\bar{\alpha}_t} (1 - \bar{\alpha}_{t-1})}{1 - \bar{\alpha}_t} \mathbf{x}_t$ and $\sigma_t^2 := \frac{1 - \bar{\alpha}_{t-1}}{1 - \bar{\alpha}_t} \beta_t$. However, \mathbf{x}_0 is intractable but can be

obtained from Gaussian denoising as implied in (2), *i.e.*,

$$\mathbf{x}_{0|t} := \frac{1}{\sqrt{\bar{\alpha}_t}} (\mathbf{x}_t - \sqrt{1 - \bar{\alpha}_t} \epsilon_{\theta}(\mathbf{x}_t; t)), \quad (4)$$

where $\epsilon_{\theta}(\mathbf{x}_t; t)$ predicts the noise in \mathbf{x}_t . By iteratively calculating \mathbf{x}_{t-1} using (3), clean images \mathbf{x}_0 can be obtained from $\mathbf{x}_T \sim \mathcal{N}(\mathbf{0}, \mathbf{I})$. DDPM can also be described by stochastic differential equations (SDE). In VP-SDE [79], the score-based diffusion models [78, 79] can be viewed as a continuous-time generalization of DDPM. They satisfy the following equation

$$\nabla_{\mathbf{x}_t} \log p_t(\mathbf{x}_t) \simeq \mathbf{s}_{\theta}(\mathbf{x}_t, t) \simeq -\frac{\epsilon_{\theta}(\mathbf{x}_t, t)}{\sqrt{1 - \bar{\alpha}_t}}, \quad (5)$$

where score function $\mathbf{s}_{\theta}(\mathbf{x}_t, t)$ models $\nabla_{\mathbf{x}} \log p_t(\mathbf{x})$ with score matching methods [40, 78]. The details of this section are provided in the supplementary.

Diffusion Model-based Image Restoration. In generation tasks, one only needs to train $\nabla_{\mathbf{x}_t} \log p_t(\mathbf{x}_t)$ (*i.e.*, to train $\epsilon_{\theta}(\mathbf{x}_t, t)$) to execute the reverse process. Assuming the availability of problem-specific scores for all noise levels, *i.e.*, $\nabla_{\mathbf{x}_t} \log p_t(\mathbf{x}_t | \mathbf{y})$, diffusion models can address IR tasks via (3). For problem-specific DMIR, we can directly train $\nabla_{\mathbf{x}_t} \log p_t(\mathbf{x}_t | \mathbf{y})$ (*i.e.*, train $\epsilon_{\theta}(\mathbf{x}_t, \mathbf{y}, t)$). However, for problem-agnostic DMIR, the problem-specific scores can be decomposed using Bayes' theorem [21, 77]

$$\nabla_{\mathbf{x}_t} \log p_t(\mathbf{x}_t | \mathbf{y}) = \nabla_{\mathbf{x}_t} \log p_t(\mathbf{x}_t) + \nabla_{\mathbf{x}_t} \log p_t(\mathbf{y} | \mathbf{x}_t), \quad (6)$$

where the first term can be approximated by the score network $\mathbf{s}_{\theta}(\mathbf{x}_t, t)$ using (5) [81], and the second term acts as a guidance component, denoting the score of $p_t(\mathbf{y} | \mathbf{x}_t)$.

Although $\nabla_{\mathbf{x}_t} \log p_t(\mathbf{y} | \mathbf{x}_t)$ is intractable in problem-agnostic DMIR, this time-dependent likelihood can be approximated through various methodologies. We summarize these approaches in Section 4.

4. Elucidating the Design Space of Guidance

In this section, we unify previous problem-agnostic DMIR methods within a common framework, demonstrating that, despite being motivated by different theories, the resulting algorithms show minor differences. We include detailed explanation of this section in the supplementary.

In the case of VP-SDE or DDPM sampling, $p_{\theta}(\mathbf{x}_0 | \mathbf{x}_t)$ has the unique posterior mean

$$\mathbf{x}_{0|t} := \mathbb{E}[\mathbf{x}_0 | \mathbf{x}_t] = \frac{1}{\sqrt{\bar{\alpha}_t}} (\mathbf{x}_t + (1 - \bar{\alpha}_t) \nabla_{\mathbf{x}_t} \log p_t(\mathbf{x}_t)). \quad (7)$$

By plugging (5) into (7), one can retrieve the empirical Bayes optimal posterior mean [21, 46, 79] $\mathbf{x}_{0|t}$ from $p_{\theta}(\mathbf{x}_0 | \mathbf{x}_t)$ using either $\mathbf{s}_{\theta}(\mathbf{x}_t, t)$ or $\epsilon_{\theta}(\mathbf{x}_t, t)$.

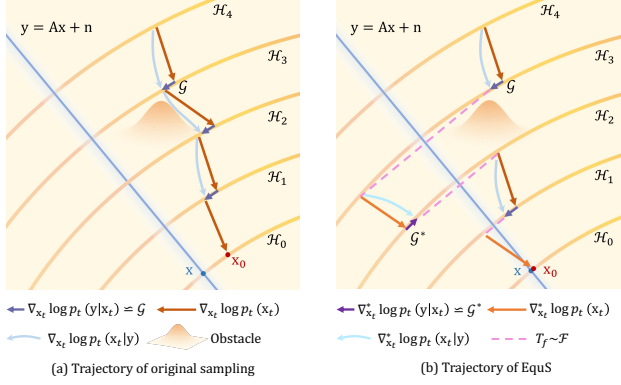


Figure 3. Conceptual illustration of the trajectories of two different sampling processes. \mathcal{H} represents the contours of the data distribution. EquS enables dual-trajectory sampling, determining \mathbf{x}_0 by considering bidirectional information.

In DMIR, one can obtain the posterior mean $\tilde{\mathbf{x}}_{0|t}$ by replacing $\nabla_{\mathbf{x}_t} \log p(\mathbf{x}_t)$ with $\nabla_{\mathbf{x}_t} \log p(\mathbf{x}_t|\mathbf{y})$ in (7), *i.e.*,

$$\tilde{\mathbf{x}}_{0|t} := \mathbb{E}[\mathbf{x}_0|\mathbf{x}_t, \mathbf{y}] = \frac{1}{\sqrt{\bar{\alpha}_t}}(\mathbf{x}_t + (1 - \bar{\alpha}_t)\nabla_{\mathbf{x}_t} \log p_t(\mathbf{x}_t|\mathbf{y})). \quad (8)$$

However, we only have $\nabla_{\mathbf{x}_t} \log p_t(\mathbf{x}_t)$ in problem-agnostic DMIR, thus to approximate $\nabla_{\mathbf{x}_t} \log p_t(\mathbf{y}|\mathbf{x}_t)$ in (6), various methods can be broadly classified into

$$\nabla_{\mathbf{x}_t} \log p_t(\mathbf{y}|\mathbf{x}_t) \simeq \mathbf{A}^\dagger(\mathbf{y} - \mathbf{A}\mathbf{x}_{0|t}), \quad (9)$$

$$\simeq \mathbf{A}^\top(\mathbf{y} - \mathbf{A}\mathbf{x}_{0|t}). \quad (10)$$

where \mathbf{A}^\dagger denotes the pseudo-inverse of \mathbf{A} , \mathbf{A}^\top represents the transpose of \mathbf{A} .

Problem-agnostic DMIR can be considered¹ as first obtaining $\mathbf{x}_{0|t}$ based on (7), and then correcting it by adding guidance ((9) or (10)), *i.e.*,

$$\tilde{\mathbf{x}}_{0|t} = \underbrace{\frac{1}{\sqrt{\bar{\alpha}_t}}(\mathbf{x}_t + (1 - \bar{\alpha}_t)\nabla_{\mathbf{x}_t} \log p_t(\mathbf{x}_t))}_{\text{original } \mathbf{x}_{0|t} \text{ in (7)}} + \underbrace{\nabla_{\mathbf{x}_t} \log p_t(\mathbf{y}|\mathbf{x}_t)}_{\text{guidance}}. \quad (11)$$

In Figure 3 (a), we show a conceptual illustration of the trajectory of this sampling process. To further promote IR performance, these methods [2, 21, 23, 77] consider computing Jacobian-vector products for (9) and (10), which can be implemented by backpropagation as $\nabla_{\mathbf{x}_t} \|\mathbf{y} - \mathbf{A}\mathbf{x}_{0|t}\|_2^2$ [21]. Unfortunately, while they sometimes improve the performance of IR, they also bring a higher computational burden due to the need for backpropagation.

¹We disregard the predefined terms preceding $\nabla_{\mathbf{x}_t} \log p_t(\mathbf{y}|\mathbf{x}_t)$.

5. Equivariant Sampling

Images are often assumed to possess certain invariance properties concerning specific transformation groups, including rotations, translations, and reflections. Intuitively, if an algorithm can reconstruct an image from a degraded image, it should similarly reconstruct the image from a transformed version of that degraded image. In this section, we illustrate how to integrate this concept into DMIR.

We denote the inverse mapping in (7) as $\mathbf{x}_{0|t} = \mathcal{D}_\theta(\mathbf{x}_t)$. The guidance in Section 4 ensures data consistency in the measurement domain

$$\mathbf{y} - \mathbf{A}\mathbf{x}_{0|t} = \mathbf{y} - \mathbf{A}\mathcal{D}_\theta(\mathbf{x}_t), \quad (12)$$

which allows us to solve the problem in (1).

Invariant Set. For a group of transformations $\mathcal{F} = \{f_1, \dots, f_{|\mathcal{F}|}\}$ which is composed of unitary matrices $T_f \in \mathbb{R}^{n \times n}$, \mathcal{X} is an invariant set when $T_f x \in \mathcal{X}$ holds for $\forall x \in \mathcal{X}$ and $\forall f \in \mathcal{F}$ [14–16].

Equivariant Inverse Mapping. We say that \mathcal{D}_θ is equivariant to the transformation group \mathcal{F} if

$$\mathcal{D}_\theta(T_f \mathbf{x}_t) = T_f \mathcal{D}_\theta(\mathbf{x}_t), \quad (13)$$

for all \mathbf{x}_t and $f \in \mathcal{F}$. Using this property, we can get the equivariant inverse mapping, *i.e.*,

$$\mathbf{x}_{0|t}^* := T_f^{-1} \mathcal{D}_\theta(T_f \mathbf{x}_t), \quad (14)$$

where T_f^{-1} represents the inverse transformation of T_f . $\nabla_{\mathbf{x}_t}^* \log p_t(\mathbf{y}|\mathbf{x}_t)$, $\nabla_{\mathbf{x}_t}^* \log p_t(\mathbf{x}_t)$, and $\nabla_{\mathbf{x}_t}^* \log p_t(\mathbf{x}_t|\mathbf{y})$ can also be computed using (9) or (10), (5) and (6), respectively. We leave the details in the supplementary.

Equivariant Sampling. A straightforward method is to average the equivariant inverse mapping in (14) over the transformation group \mathcal{F} . However, for large groups and in light of the lengthy sampling steps in diffusion models, this approach introduces significant computational overhead, diminishing algorithmic practicality. To mitigate this, we propose **Equivariant Sampling (EquS)** as an efficient estimate of the averaged equivariant inverse mapping. For simplification, we use $p_\theta(\mathbf{x}_{t-1}|\mathbf{x}_t, \mathbf{x}_{0|t}, \mathbf{y})$ to represent the composition of (11) and (3). EquS first performs a standard reverse process (first $\mathcal{D}_\theta(\mathbf{x}_t)$, then $p_\theta(\mathbf{x}_{t-1}|\mathbf{x}_t, \mathbf{x}_{0|t}, \mathbf{y})$), followed by an equivariant reverse process (first $T_f^{-1} \mathcal{D}_\theta(T_f \mathbf{x}_t)$, then $p_\theta(\mathbf{x}_{t-1}|\mathbf{x}_t, \mathbf{x}_{0|t}^*, \mathbf{y})$). This whole process is illustrated in Figure 4. It is worth noting that EquS requires no additional NFEs or hyperparameters.

Equivariant Sampling from a Loss Perspective. With the equivariant inverse mapping, we could rewrite (12) as

$$\mathbf{y} - \mathbf{A}T_f^{-1} \mathcal{D}_\theta(T_f \mathbf{x}_t) = \mathbf{y} - \mathbf{A}_f \mathcal{D}_\theta(\tilde{\mathbf{x}}_t), \quad (15)$$

where $\mathbf{A}_f = \mathbf{A} \circ T_f^{-1}$ and $\tilde{\mathbf{x}}_t = T_f \mathbf{x}_t$.

² \circ denotes the composition of two functions

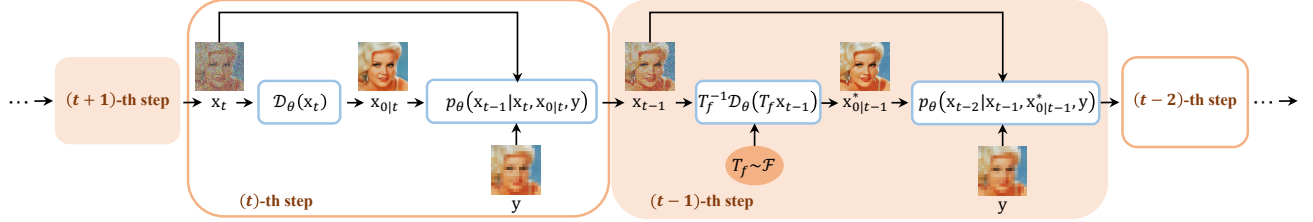


Figure 4. The sampling process of the **Equivariant Sampling (EquS)**.

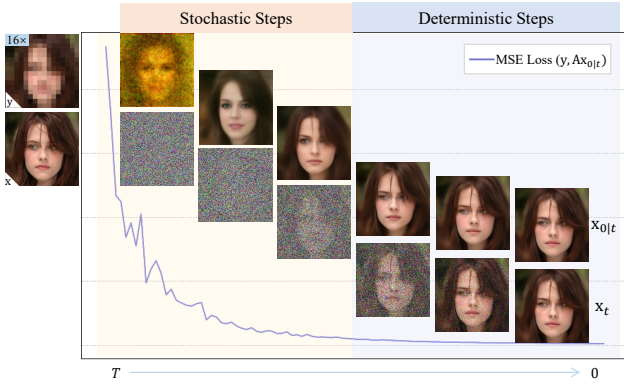


Figure 5. Deconstruction of the diffusion reverse process: stochastic steps and deterministic steps. $\mathbf{x}_{0|t}$ is more certain in the deterministic steps.

We can see that EquS introduces a new loss term $\|\mathbf{y} - \mathbf{A}_f \mathcal{D}_\theta(\tilde{\mathbf{x}}_t)\|_2^2$ for the IR problem in (1), provided that \mathbf{A} itself is not invariant under all T_f^{-1} . During the diffusion reverse iteration, EquS minimizes not only $\|\mathbf{y} - \mathbf{A} \mathcal{D}_\theta(\mathbf{x}_t)\|_2^2$ but also $\|\mathbf{y} - \mathbf{A}_f \mathcal{D}_\theta(\tilde{\mathbf{x}}_t)\|_2^2$. This addition enhances the accuracy of the final reconstructed output by imposing a new constraint, which requires that the ultimate output maintains equivariance under the transformation group during the algorithmic iteration process.

We show a conceptual illustration of the trajectory of EquS in Figure 3 (b). EquS enables dual-trajectory sampling (trajectory of the standard reverse process and trajectory of the equivariant reverse process), determining the reconstructed image \mathbf{x}_0 by considering equivariant information.

5.1. Sampling Scheme

Sampling Process Deconstruction. As shown in Figure 5, the mean square error between $\mathbf{A}\mathbf{x}_{0|t}$ and \mathbf{y} in stochastic steps is larger than that in the deterministic steps. This suggests that $\mathbf{x}_{0|t}$ is more certain in the deterministic steps. Another interesting view is that we can interpret the sampling process in DMIR as a structured sequence, *i.e.*, initially mitigating residuals, followed by noise reduction [58].

Uniform Schedule Sampling. Most DMIR methods [35,

44, 77, 88] consider DDIM [76] to accelerate the sampling. The whole sampling could be written as the form in (1), *i.e.*,

$$\hat{\mathbf{x}} = \arg \min_{\mathbf{x}} \sum_{t \in S} \|\mathbf{y} - \mathbf{A}\mathbf{x}_{0|t}\|_2^2, \quad (16)$$

where $\|\mathbf{y} - \mathbf{A}\mathbf{x}_{0|t}\|_2^2$ comes from the guidance in Section 4 [35], S is a sub-sequence of $[1, \dots, T]$. However, constructing S using a uniform schedule results in equal weights for the stochastic and deterministic steps. Since the term $\|\mathbf{y} - \mathbf{A}\mathbf{x}_{0|t}\|_2^2$ in the stochastic steps is large, this causes the summation term in (16) to become excessively large, thus increasing the difficulty of reconstruction.

Timestep-Aware Schedule Based on the previous paragraph, giving more weight to the deterministic steps can reduce the summation term in (16), thereby introducing more deterministic information and improving the overall efficiency of the sampling process³. Intuitively, this approach allows for finer detail refinement when $\mathbf{x}_{0|t}$ is deterministic. We refer to this kind of schedule, which gives more weight to the deterministic steps, as **Timestep-Aware Schedule (TAS)**, and the version of EquS integrated with TAS is termed as EquS⁺.

6. Experiments

6.1. Experiment Details

Experiment Settings. We evaluate EquS and EquS⁺ across a range of typical IR tasks, including compressed sensing (CS), inpainting, super-resolution (SR), deblurring, and colorization. For validation, we use the ImageNet 1K [26] and CelebA 1K [42] datasets, with images resized to 256×256. To ensure fair comparisons, we apply the same pre-trained diffusion models across all methods: [27] for ImageNet and [60] for CelebA-HQ. All experiments were performed on NVIDIA GeForce RTX 4090. During implementation, EquS uses horizontal flipping to construct \mathcal{F} , while TAS employs a quadratic sampling schedule without altering the length of the sub-sequence S . We append a suffix to the method name when incorporating our approach. Due to

³During implementation, this can be achieved by constructing S , *e.g.*, using a quadratic schedule.

ImageNet	Gaussian Deblurring	Block-based CS 25%	Inpainting	4× Bicubic SR	Colorization
Method	PSNR↑/SSIM↑/LPIPS↓	PSNR↑/SSIM↑/LPIPS↓	PSNR↑/SSIM↑/LPIPS↓	PSNR↑/SSIM↑/LPIPS↓	Cons↓/FID↓/LPIPS↓
A[†]y	18.57 / 0.586 / 0.376	12.83 / 0.192 / 0.724	14.62 / 0.661 / 0.413	26.27 / 0.771 / 0.302	53.92 / 44.95 / 0.167
DPS [21]	26.12 / 0.729 / 0.341	30.61 / 0.868 / 0.170	35.56 / 0.964 / 0.052	22.49 / 0.584 / 0.468	619.3 / 54.78 / 0.277
IIGDM [77]	42.19 / 0.980 / 0.035	30.61 / 0.867 / 0.170	35.54 / 0.964 / 0.052	27.89 / 0.815 / 0.217	177.3 / 36.75 / 0.194
DeqIR [12]	43.57 / 0.986 / 0.017	25.26 / 0.696 / 0.296	32.36 / 0.956 / 0.036	26.90 / 0.788 / 0.250	25.26 / 39.05 / 0.176
CDDB [23]	26.42 / 0.750 / 0.311	28.60 / 0.795 / 0.225	34.92 / 0.968 / 0.026	23.47 / 0.630 / 0.423	275.1 / 39.04 / 0.183
CDDB-EquS⁺	27.55 / 0.797 / 0.268	32.05 / 0.890 / 0.099	36.18 / 0.976 / 0.020	25.41 / 0.712 / 0.358	114.0 / 41.18 / 0.168
DDRM [44]	43.01 / 0.986 / 0.014	27.54 / 0.766 / 0.276	34.60 / 0.965 / 0.030	27.39 / 0.801 / 0.241	144.4 / 36.77 / 0.162
DDRM-EquS⁺	44.69 / 0.990 / 0.010	31.70 / 0.886 / 0.109	35.93 / 0.973 / 0.025	27.54 / 0.807 / 0.248	142.9 / 39.70 / 0.162
DDNM [88]	44.94 / 0.990 / 0.011	28.59 / 0.795 / 0.225	34.93 / 0.968 / 0.025	27.45 / 0.801 / 0.231	21.92 / 36.87 / 0.157
DDNM-EquS⁺	46.99 / 0.993 / 0.006	31.87 / 0.887 / 0.103	36.13 / 0.976 / 0.021	27.63 / 0.809 / 0.242	21.68 / 39.34 / 0.158

CelebA	Gaussian Deblurring	Block-based CS 25%	Inpainting	4× Bicubic SR	Colorization
Method	PSNR↑/SSIM↑/LPIPS↓	PSNR↑/SSIM↑/LPIPS↓	PSNR↑/SSIM↑/LPIPS↓	PSNR↑/SSIM↑/LPIPS↓	Cons↓/FID↓/LPIPS↓
A[†]y	18.85 / 0.686 / 0.305	12.11 / 0.155 / 0.790	14.65 / 0.653 / 0.459	30.64 / 0.881 / 0.214	54.86 / 46.65 / 0.138
DPS [21]	30.65 / 0.856 / 0.173	34.02 / 0.919 / 0.122	37.80 / 0.967 / 0.061	26.83 / 0.778 / 0.229	578.0 / 42.33 / 0.160
IIGDM [77]	40.19 / 0.975 / 0.051	34.02 / 0.919 / 0.122	37.80 / 0.966 / 0.061	31.80 / 0.890 / 0.124	353.5 / 33.32 / 0.103
DeqIR [12]	46.85 / 0.992 / 0.011	32.56 / 0.894 / 0.120	38.22 / 0.979 / 0.019	31.82 / 0.892 / 0.125	72.16 / 32.93 / 0.201
CDDB [23]	30.86 / 0.862 / 0.161	33.51 / 0.907 / 0.111	39.36 / 0.982 / 0.017	27.20 / 0.789 / 0.219	347.8 / 32.25 / 0.123
CDDB-EquS⁺	32.60 / 0.898 / 0.162	34.78 / 0.927 / 0.091	39.82 / 0.983 / 0.016	30.16 / 0.855 / 0.209	235.4 / 32.43 / 0.110
DDRM [44]	43.07 / 0.985 / 0.023	32.50 / 0.896 / 0.128	38.30 / 0.973 / 0.035	31.63 / 0.886 / 0.123	170.6 / 31.20 / 0.105
DDRM-EquS⁺	43.15 / 0.986 / 0.023	34.47 / 0.925 / 0.103	38.69 / 0.975 / 0.034	32.39 / 0.901 / 0.134	169.4 / 31.20 / 0.102
DDNM [88]	46.73 / 0.992 / 0.011	33.51 / 0.907 / 0.111	39.37 / 0.982 / 0.017	31.64 / 0.885 / 0.116	28.49 / 26.19 / 0.090
DDNM-EquS⁺	46.88 / 0.993 / 0.010	34.76 / 0.926 / 0.091	39.85 / 0.983 / 0.016	32.44 / 0.901 / 0.126	31.01 / 26.08 / 0.086

Table 1. Quantitative results of zero-shot DMIR methods on **ImageNet**(*top*) and **CelebA**(*bottom*), including five typical IR tasks. The enhanced versions show improved quantitative performance over their original counterparts.

space constraints, additional details on the experiments can be found in the Supplementary.

Evaluation Metrics. We employ PSNR, SSIM [89], and LPIPS [104] as the main evaluation metrics for most IR tasks. For colorization specifically, we utilize the Consistency metric (referred to as *Cons*) [88] along with FID [38], since PSNR and SSIM do not adequately capture performance in this context. Generally, improved performance is indicated by higher PSNR and SSIM values, alongside lower values for LPIPS, FID, and *Cons*.

6.2. Evaluation on Different IR Tasks

We compare our method against SOTA zero-shot DMIR methods, including DPS [21], DDRM [44], DDNM [88], IIGDM [77], CDDB [12], and DeqIR [12]. EquS⁺ is integrated into DDRM, CDDB, and DDNM. We evaluate under five typical IR tasks: block-based CS at a 0.25 compression ratio, text mask for inpainting, 4× bicubic downsampling for SR, Gaussian blur for deblurring, and average grayscale operator for colorization. A[†]y are used as baselines.

Additional quantitative and qualitative results, including varying degrees of deconstruction and different IR tasks (*e.g.*, Walsh-Hadamard CS, anisotropic blur), are provided in the Supplementary.

The Effect of Our Method. We show the quantitative results of zero-shot DMIR methods in Table 1.

The enhanced versions show improved performance over their original counterparts. In Figure 1, we show that our method offers better quantitative performance and improved qualitative results. For example, on the ImageNet for the Gaussian deblurring task, DDNM-EquS⁺ achieved a significant performance boost over DDNM, with a notable 2.05 dB increase in PSNR and a 0.005 improvement in LPIPS; On the ImageNet for block-based CS task, CDDB-EquS⁺ achieves a PSNR improvement of 3.45 dB and an LPIPS improvement of 0.126 compared to CDDB. By utilizing dual-trajectory sampling and TAS, EquS⁺ significantly enhances previous SOTA methods, demonstrating both the effectiveness (in quantitative performance improvement) and versatility (across various IR tasks) of our method.

Quantitative and Qualitative Results. CS. CDDB-EquS⁺ outperforms most other methods on benchmarks. Compared to the competitive IR method IIGDM, CDDB-EquS⁺ achieves an LPIPS improvement of up to 0.071 and a PSNR gain of up to 1.44 dB on ImageNet. For qualitative results, as shown in Figure 6, the enhanced versions demonstrate enhanced visual quality with finely restored details of animal fur. These visual comparisons align closely with

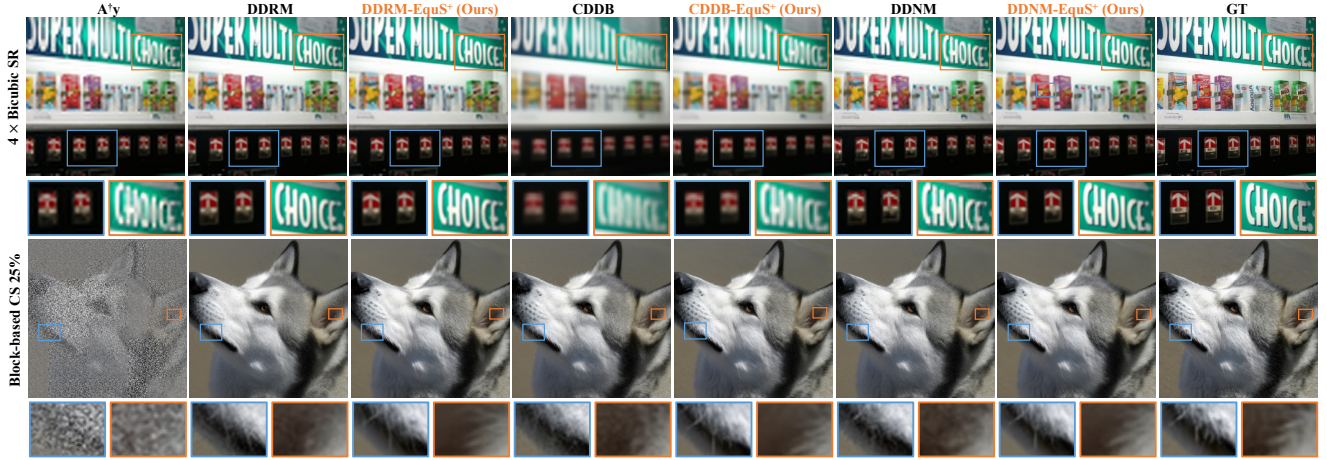


Figure 6. Qualitative results of zero-shot DMIR methods. A clearer text (*top*) and the fur of the animals (*bottom*) can be observed.

the quantitative findings, underscoring the effectiveness of our approach. **Deblurring.** Notably, DDNM-EquS⁺ outperforms most other methods on benchmarks. **Inpainting.** CDDB-EquS⁺ outperforms most other methods on benchmarks. For instance, compared to the competitive IR method DPS, CDDB-EquS⁺ achieves an LPIPS improvement of up to 0.031 and a PSNR gain of up to 0.57 dB on ImageNet. **SR.** DDNM-EquS⁺ outperforms most other methods on CelebA. Although IIGDM achieves superior performance on the ImageNet dataset, its reliance on gradient computation introduces additional computational overhead. For qualitative results, as shown in Figure 6, the enhanced versions demonstrate better visual quality, capturing more legible text. Our method achieves substantial performance gains without additional computational cost. **Colorization.** In Table 1, the enhanced versions show competitive performance, which implies that there exists an inevitable trade-off between distortion (*Cons*) and perception (FID, LPIPS) [5] in colorization. In Figure 1, we further show that our method is adaptable to various IR applications, robust to different scales, and resilient to different noise levels. Due to space constraints, we provided more qualitative results in the Supplementary.

6.3. Robustness in Noisy IR Tasks

We also performed a comparison with DDPG [35], a SOTA zero-shot DMIR method for deblurring and SR, and validated the robustness of the proposed EquS under varying noise intensities. In Table 2, we show quantitative results on CelebA-HQ. DDPG-EquS achieves better quantitative results than DDPG. These results indicate that EquS demonstrates stability across varying noise intensities.

Moreover, we validate EquS on DDNM⁺ [88], a method that can handle noisy IR tasks. We present the quantitative results on ImageNet in Table 3. EquS significantly improves quantitative performance, such as achieving a 36.34

CelebA		A†y	DDPG [35]	DDPG-EquS
Task	σ_y	PSNR↑/SSIM↑/LPIPS↓	PSNR↑/SSIM↑/LPIPS↓	PSNR↑/SSIM↑/LPIPS↓
GD	0	36.58 / 0.934 / 0.124	47.76 / 0.995 / 0.006	47.77 / 0.995 / 0.006
	0.01	22.83 / 0.514 / 0.410	33.06 / 0.903 / 0.113	33.14 / 0.904 / 0.112
	0.05	19.74 / 0.306 / 0.552	31.22 / 0.868 / 0.144	31.32 / 0.870 / 0.143
	0.10	17.79 / 0.201 / 0.623	29.94 / 0.823 / 0.180	30.04 / 0.825 / 0.179
MD	0.01	21.77 / 0.486 / 0.461	32.54 / 0.890 / 0.126	32.60 / 0.891 / 0.125
	0.05	17.17 / 0.206 / 0.638	29.01 / 0.817 / 0.177	29.17 / 0.821 / 0.175
	0.10	18.85 / 0.686 / 0.305	27.71 / 0.779 / 0.200	27.91 / 0.785 / 0.197
SR	0	29.77 / 0.862 / 0.233	31.59 / 0.886 / 0.120	31.73 / 0.888 / 0.119
	0.01	29.28 / 0.828 / 0.260	31.81 / 0.882 / 0.154	31.91 / 0.883 / 0.154
	0.05	24.83 / 0.560 / 0.469	29.39 / 0.828 / 0.188	29.52 / 0.831 / 0.187

Table 2. Quantitative results of noisy IR tasks on CelebA-HQ. σ_y denotes the noise level. “GD” represents Gaussian Deblurring, “MD” represents Motion Deblurring, and “SR” represents 4× Bicubic SR. We use **bold** to indicate improved scores and underline to represent results that match previous methods.

ImageNet		A†y	DDNM ⁺ [88]	DDNM ⁺ -EquS
Task		PSNR↑/SSIM↑/LPIPS↓	PSNR↑/SSIM↑/LPIPS↓	PSNR↑/SSIM↑/LPIPS↓
CS		14.22 / 0.154 / 0.680	20.68 / 0.588 / 0.418	21.22 / 0.604 / 0.412
SR		14.33 / 0.149 / 0.749	22.66 / 0.604 / 0.420	25.71 / 0.724 / 0.329
		<i>Cons.</i> ↓/FID↓/LPIPS↓	<i>Cons.</i> ↓/FID↓/LPIPS↓	<i>Cons.</i> ↓/FID↓/LPIPS↓
Colorization		9376 / 239.4 / 0.750	3362 / 125.1 / 0.574	1969 / 88.76 / 0.395

Table 3. Quantitative results of noisy IR tasks on ImageNet. Noise level is 0.2. We use **bold** to indicate improved scores. “CS” represents Walshhadamard CS 25%, and “SR” represents 4× Average Pooling SR.

improvement in FID for colorization compared to DDNM⁺. In Figure 8, DDNM⁺-EquS achieves better visual quality. Note that EquS can be seamlessly incorporated into previous methods without adding extra computational costs.

6.4. Test on other cases

Inpainting with Black Hole Mask. To further demonstrate the robustness of the method, we experimented with two black hole masks in inpainting. The quantitative results are

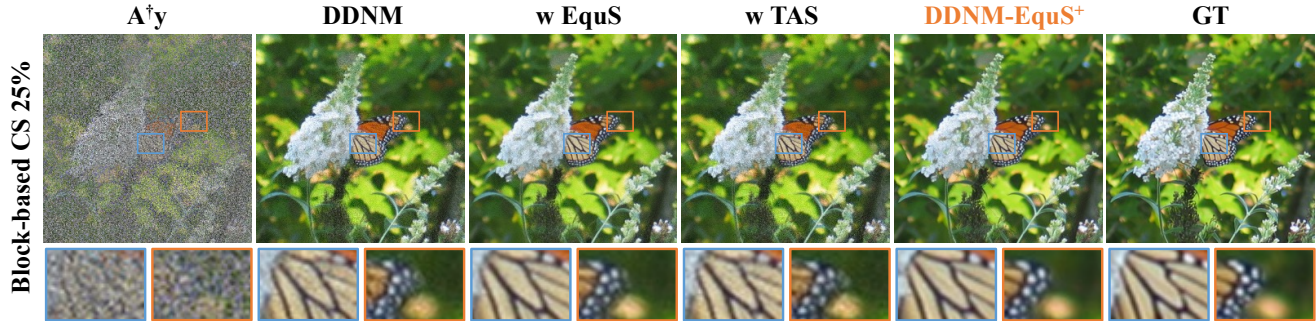


Figure 7. Qualitative results of ablation studies. The final version reveals clearer textures of the butterfly wings.

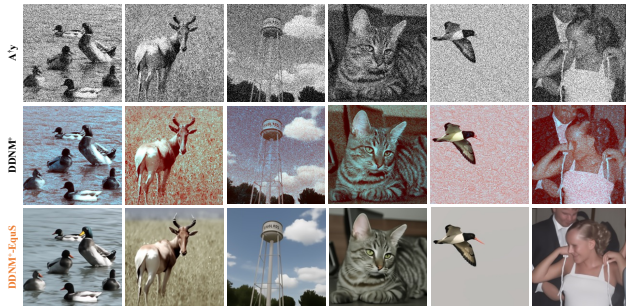


Figure 8. Qualitative results of colorization on Imagenet. Our method enables better visual quality.

CelebA	DDNM [88]	DDNM-EquS ⁺
Inpainting	PSNR \uparrow /SSIM \uparrow /LPIPS \downarrow	PSNR \uparrow /SSIM \uparrow /LPIPS \downarrow
Square	35.29 / 0.977 / 0.018	36.33 / 0.981 / 0.017
Circle	33.61 / 0.971 / 0.022	34.61 / 0.975 / 0.021

Table 4. Quantitative results on ImageNet. We use **bold** to indicate improved scores. Our method is robust in these situations.

shown in Table 4. Our method is robust in these situations.

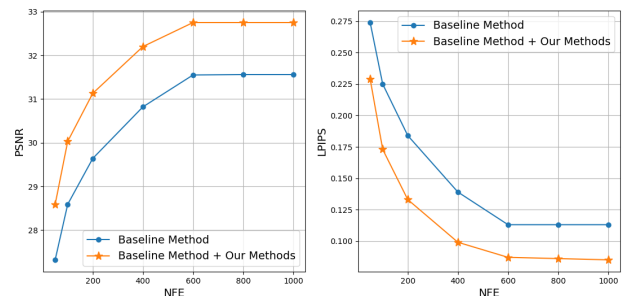
6.5. Ablation Studies

Proposed Methods. To demonstrate the effect of our proposed EquS and TAS, we performed ablation studies using DDNM [88] as a baseline. The quantitative results shown in Table 5 highlight the benefits of the proposed EquS and TAS, resulting in consistent improvements in various IR tasks. We present qualitative results of ablation studies in Figure 7, showing that EquS⁺ captures finer texture details. In summary, both EquS and EquS⁺ have two notable advantages: (1) compatibility with previous methods and (2) no additional computational overhead. Further ablation studies on more IR tasks are available in the Supplementary.

NFE vs. Evaluation Metrics. In Figure 9, it can be seen that our method consistently improves the quantitative results under different NFE conditions. This indicates that

ImageNet	Gaussian Deblurring	Block-based CS 25%	Inpainting
EquS	TAS	PSNR \uparrow /SSIM \uparrow /LPIPS \downarrow	PSNR \uparrow /SSIM \uparrow /LPIPS \downarrow
\times	\times	44.94 / 0.990 / 0.011	28.59 / 0.795 / 0.225
\checkmark	\times	45.37 / 0.991 / 0.009	30.02 / 0.845 / 0.173
\checkmark	\checkmark	46.31 / 0.992 / 0.007	30.32 / 0.844 / 0.153
\checkmark	\checkmark	46.99 / 0.993 / 0.006	31.87 / 0.887 / 0.103
			34.93 / 0.968 / 0.025
			35.65 / 0.973 / 0.023
			35.59 / 0.972 / 0.021
			36.13 / 0.976 / 0.021

Table 5. Quantitative results of ablation studies. We use **bold** to indicate the best scores.



(a) NFE vs. PSNR (**higher** is better). (b) NFE vs. LPIPS (**lower** is better).

Figure 9. NFE vs. Evaluation metrics on block-based CS 25%. Our method is not limited by specific NFE.

our method is not limited by the number of sampling steps.

7. Conclusion

In this paper, we propose a novel zero-shot diffusion model-based IR method, called EquS. Specifically, we incorporate an equivariant inverse mapping into the sampling process and impose equivariant information through dual sampling trajectories. Additionally, we introduce TAS to prioritize deterministic steps and enhance certainty in the sampling process. With TAS, EquS⁺ further improves both the overall efficiency of the sampling chain and the IR performance. Comprehensive experiments demonstrate the outstanding performance of EquS and EquS⁺ across a range of IR tasks. Moreover, our methods can be seamlessly integrated into existing methods, boosting their performance without incurring additional computational costs.

References

- [1] Giovanni S Alberti, Ernesto De Vito, Matti Lassas, Luca Ratti, and Matteo Santacesaria. Learning the optimal tikhonov regularizer for inverse problems. *Advances in Neural Information Processing Systems*, 34:25205–25216, 2021. 3
- [2] Yaşar Utku Alçalar and Mehmet Akçakaya. Zero-shot adaptation for approximate posterior sampling of diffusion models in inverse problems. *arXiv preprint arXiv:2407.11288*, 2024. 2, 3, 4
- [3] Mark R Banham and Aggelos K Katsaggelos. Digital image restoration. *IEEE signal processing magazine*, 14(2):24–41, 1997. 2
- [4] Joshua Batson and Loic Royer. Noise2self: Blind denoising by self-supervision. In *International Conference on Machine Learning*, pages 524–533. PMLR, 2019. 2
- [5] Yochai Blau and Tomer Michaeli. The perception-distortion tradeoff. In *Proceedings of the IEEE Conference on Computer Vision and Pattern Recognition*, pages 6228–6237, 2018. 7
- [6] Jiezhong Cao, Yong Guo, Qingyao Wu, Chunhua Shen, Junzhou Huang, and Mingkui Tan. Adversarial learning with local coordinate coding. In *International Conference on Machine Learning*, pages 707–715. PMLR, 2018. 2
- [7] Jiezhong Cao, Yong Guo, Qingyao Wu, Chunhua Shen, Junzhou Huang, and Mingkui Tan. Improving generative adversarial networks with local coordinate coding. *IEEE Transactions on Pattern Analysis and Machine Intelligence*, 2020. 2
- [8] Jiezhong Cao, Yawei Li, Kai Zhang, and Luc Van Gool. Video super-resolution transformer. *arXiv preprint arXiv:2106.06847*, 2021. 2
- [9] Jiezhong Cao, Jingyun Liang, Kai Zhang, Yawei Li, Yulun Zhang, Wenguan Wang, and Luc Van Gool. Reference-based image super-resolution with deformable attention transformer. In *ECCV*, 2022. 2
- [10] Jiezhong Cao, Jingyun Liang, Kai Zhang, Wenguan Wang, Qin Wang, Yulun Zhang, Hao Tang, and Luc Van Gool. Towards interpretable video super-resolution via alternating optimization. In *ECCV*, 2022.
- [11] Jiezhong Cao, Qin Wang, Yongqin Xian, Yawei Li, Bingbing Ni, Zhiming Pi, Kai Zhang, Yulun Zhang, Radu Timofte, and Luc Van Gool. Ciaosr: Continuous implicit attention-in-attention network for arbitrary-scale image super-resolution. In *Proceedings of the IEEE/CVF Conference on Computer Vision and Pattern Recognition*, 2023. 2
- [12] Jiezhong Cao, Yue Shi, Kai Zhang, Yulun Zhang, Radu Timofte, and Luc Van Gool. Deep equilibrium diffusion restoration with parallel sampling. In *CVPR*, pages 2824–2834, 2024. 2, 3, 6
- [13] Hernan Carrillo, Michaël Clément, Aurélie Bugeau, and Edgar Simo-Serra. Diffusart: Enhancing line art colorization with conditional diffusion models. In *Proceedings of the IEEE/CVF Conference on Computer Vision and Pattern Recognition*, pages 3486–3490, 2023. 2
- [14] Dongdong Chen, Julián Tachella, and Mike E Davies. Equivariant imaging: Learning beyond the range space. In *Proceedings of the IEEE/CVF International Conference on Computer Vision*, pages 4379–4388, 2021. 2, 4
- [15] Dongdong Chen, Julián Tachella, and Mike E Davies. Robust equivariant imaging: a fully unsupervised framework for learning to image from noisy and partial measurements. In *Proceedings of the IEEE/CVF Conference on Computer Vision and Pattern Recognition*, pages 5647–5656, 2022.
- [16] Dongdong Chen, Mike Davies, Matthias J Ehrhardt, Carola-Bibiane Schönlieb, Ferdia Sherry, and Julián Tachella. Imaging with equivariant deep learning: From unrolled network design to fully unsupervised learning. *IEEE Signal Processing Magazine*, 40(1):134–147, 2023. 2, 4
- [17] Liangyu Chen, Xiaojie Chu, Xiangyu Zhang, and Jian Sun. Simple baselines for image restoration. In *ECCV*, 2022. 2
- [18] Zheng Chen, Yulun Zhang, Ding Liu, Jinjin Gu, Linghe Kong, Xin Yuan, et al. Hierarchical integration diffusion model for realistic image deblurring. *Advances in neural information processing systems*, 36, 2024. 2
- [19] Jooyoung Choi, Sungwon Kim, Yonghyun Jeong, Youngjune Gwon, and Sungroh Yoon. Ilvr: Conditioning method for denoising diffusion probabilistic models. In *ICCV*, 2021. 2
- [20] Hyungjin Chung and Jong Chul Ye. Deep diffusion image prior for efficient ood adaptation in 3d inverse problems. *arXiv preprint arXiv:2407.10641*, 2024. 3
- [21] Hyungjin Chung, Jeongsol Kim, Michael T McCann, Marc L Klasky, and Jong Chul Ye. Diffusion posterior sampling for general noisy inverse problems. In *ICLR*, 2023. 2, 3, 4, 6
- [22] Hyungjin Chung, Dohoon Ryu, Michael T McCann, Marc L Klasky, and Jong Chul Ye. Solving 3d inverse problems using pre-trained 2d diffusion models. In *Proceedings of the IEEE/CVF Conference on Computer Vision and Pattern Recognition*, pages 22542–22551, 2023. 2
- [23] Hyungjin Chung, Jeongsol Kim, and Jong Chul Ye. Direct diffusion bridge using data consistency for inverse problems. *Advances in Neural Information Processing Systems*, 36, 2024. 3, 4, 6
- [24] Ciprian Corneanu, Raghudeep Gadde, and Aleix M Martinez. Latentpaint: Image inpainting in latent space with diffusion models. In *Proceedings of the IEEE/CVF Winter Conference on Applications of Computer Vision*, pages 4334–4343, 2024. 2
- [25] Florinel-Alin Croitoru, Vlad Hondru, Radu Tudor Ionescu, and Mubarak Shah. Diffusion models in vision: A survey. *IEEE Transactions on Pattern Analysis and Machine Intelligence*, 2023. 2
- [26] Jia Deng, Wei Dong, Richard Socher, Li-Jia Li, Kai Li, and Li Fei-Fei. Imagenet: A large-scale hierarchical image database. In *Proceedings of the IEEE/CVF Conference on Computer Vision and Pattern Recognition*, 2009. 5
- [27] Prafulla Dhariwal and Alexander Nichol. Diffusion models beat gans on image synthesis. *Advances in neural information processing systems*, 34:8780–8794, 2021. 2, 5

- [28] Chao Dong, Yubin Deng, Chen Change Loy, and Xiaoou Tang. Compression artifacts reduction by a deep convolutional network. In *ICCV*, 2015. 2
- [29] Chao Dong, Chen Change Loy, Kaiming He, and Xiaoou Tang. Image super-resolution using deep convolutional networks. *IEEE Transactions on Pattern Analysis and Machine Intelligence*, 2015. 2
- [30] Runmin Dong, Shuai Yuan, Bin Luo, Mengxuan Chen, Jinxiao Zhang, Lixian Zhang, Weijia Li, Juepeng Zheng, and Haohuan Fu. Building bridges across spatial and temporal resolutions: Reference-based super-resolution via change priors and conditional diffusion model. In *Proceedings of the IEEE/CVF Conference on Computer Vision and Pattern Recognition*, pages 27684–27694, 2024. 2
- [31] Zehao Dou and Yang Song. Diffusion posterior sampling for linear inverse problem solving: A filtering perspective. In *The Twelfth International Conference on Learning Representations*, 2024. 2
- [32] Xueyang Fu, Menglu Wang, Xiangyong Cao, Xinghao Ding, and Zheng-Jun Zha. A model-driven deep unfolding method for jpeg artifacts removal. *TNNLS*, 2021. 2
- [33] Kanchana Vaishnavi Gandikota and Paramanand Chandramouli. Text-guided explorable image super-resolution. In *Proceedings of the IEEE/CVF Conference on Computer Vision and Pattern Recognition*, pages 25900–25911, 2024. 3
- [34] Sicheng Gao, Xuhui Liu, Bohan Zeng, Sheng Xu, Yanjing Li, Xiaoyan Luo, Jianzhuang Liu, Xiantong Zhen, and Baochang Zhang. Implicit diffusion models for continuous super-resolution. In *Proceedings of the IEEE/CVF conference on computer vision and pattern recognition*, pages 10021–10030, 2023. 2
- [35] Tomer Garber and Tom Tirer. Image restoration by denoising diffusion models with iteratively preconditioned guidance. In *Proceedings of the IEEE/CVF Conference on Computer Vision and Pattern Recognition*, pages 25245–25254, 2024. 2, 3, 5, 7
- [36] Ian Goodfellow, Jean Pouget-Abadie, Mehdi Mirza, Bing Xu, David Warde-Farley, Sherjil Ozair, Aaron Courville, and Yoshua Bengio. Generative adversarial nets. *Advances in neural information processing systems*, 27, 2014. 2
- [37] Ishaan Gulrajani, Faruk Ahmed, Martin Arjovsky, Vincent Dumoulin, and Aaron Courville. Improved training of wasserstein gans. In *Advances in Neural Information Processing Systems*, 2017. 2
- [38] Martin Heusel, Hubert Ramsauer, Thomas Unterthiner, Bernhard Nessler, and Sepp Hochreiter. Gans trained by a two time-scale update rule converge to a local nash equilibrium. In *Advances in Neural Information Processing Systems*, 2017. 6
- [39] Jonathan Ho, Ajay Jain, and Pieter Abbeel. Denoising diffusion probabilistic models. In *Advances in Neural Information Processing Systems*, 2020. 2, 3
- [40] Aapo Hyvärinen and Peter Dayan. Estimation of non-normalized statistical models by score matching. *Journal of Machine Learning Research*, 6(4), 2005. 3
- [41] Xixi Jia, Sanyang Liu, Xiangchu Feng, and Lei Zhang. Focnet: A fractional optimal control network for image denoising. In *Proceedings of the IEEE/CVF Conference on Computer Vision and Pattern Recognition*, 2019. 2
- [42] Tero Karras, Timo Aila, Samuli Laine, and Jaakko Lehtinen. Progressive growing of GANs for improved quality, stability, and variation. In *International conference on machine learning*, 2018. 5
- [43] Bahjat Kawar, Gregory Vaksman, and Michael Elad. Snips: Solving noisy inverse problems stochastically. *Advances in Neural Information Processing Systems*, 2021. 3
- [44] Bahjat Kawar, Michael Elad, Stefano Ermon, and Jiaming Song. Denoising diffusion restoration models. In *Advances in Neural Information Processing Systems*, 2022. 2, 3, 5, 6
- [45] Jiwon Kim, Jung Kwon Lee, and Kyoung Mu Lee. Accurate image super-resolution using very deep convolutional networks. In *Proceedings of the IEEE/CVF Conference on Computer Vision and Pattern Recognition*, 2016. 2
- [46] Kwanyoung Kim and Jong Chul Ye. Noise2score: tweedie’s approach to self-supervised image denoising without clean images. *Advances in Neural Information Processing Systems*, 34:864–874, 2021. 2, 3
- [47] Yoonsik Kim, Jae Woong Soh, Jaewoo Park, Byeongyong Ahn, Hyun-Seung Lee, Young-Su Moon, and Nam Ik Cho. A pseudo-blind convolutional neural network for the reduction of compression artifacts. *TCSVT*, 2019. 2
- [48] Alexander Krull, Tim-Oliver Buchholz, and Florian Jug. Noise2void-learning denoising from single noisy images. In *Proceedings of the IEEE/CVF conference on computer vision and pattern recognition*, pages 2129–2137, 2019. 2
- [49] Sojin Lee, Dogyun Park, Inho Kong, and Hyunwoo J Kim. Diffusion prior-based amortized variational inference for noisy inverse problems. *arXiv preprint arXiv:2407.16125*, 2024. 2
- [50] Jaakko Lehtinen, Jacob Munkberg, Jon Hasselgren, Samuli Laine, Tero Karras, Miika Aittala, and Timo Aila. Noise2noise: Learning image restoration without clean data. *arXiv preprint arXiv:1803.04189*, 2018. 2
- [51] Guangyuan Li, Chen Rao, Juncheng Mo, Zhanjie Zhang, Wei Xing, and Lei Zhao. Rethinking diffusion model for multi-contrast mri super-resolution. In *Proceedings of the IEEE/CVF Conference on Computer Vision and Pattern Recognition*, pages 11365–11374, 2024. 2
- [52] Haoying Li, Yifan Yang, Meng Chang, Shiqi Chen, Huajun Feng, Zhihai Xu, Qi Li, and Yueting Chen. Srdiff: Single image super-resolution with diffusion probabilistic models. *Neurocomputing*, 479:47–59, 2022. 2
- [53] Wenbo Li, Zhe Lin, Kun Zhou, Lu Qi, Yi Wang, and Jiaya Jia. Mat: Mask-aware transformer for large hole image inpainting. In *Proceedings of the IEEE/CVF Conference on Computer Vision and Pattern Recognition*, 2022. 2
- [54] Jingyun Liang, Jiezhong Cao, Yuchen Fan, Kai Zhang, Rakesh Ranjan, Yawei Li, Radu Timofte, and Luc Van Gool. Vrt: A video restoration transformer. *TIP*, 2024. 2
- [55] Wei-An Lin, Haofu Liao, Cheng Peng, Xiaohang Sun, Jingdan Zhang, Jiebo Luo, Rama Chellappa, and Shao-hua Kevin Zhou. Dudonet: Dual domain network for ct

- metal artifact reduction. In *Proceedings of the IEEE/CVF Conference on Computer Vision and Pattern Recognition*, pages 10512–10521, 2019. 2
- [56] Xinqi Lin, Jingwen He, Ziyang Chen, Zhaoyang Lyu, Ben Fei, Bo Dai, Wanli Ouyang, Yu Qiao, and Chao Dong. Diffbir: Towards blind image restoration with generative diffusion prior. *arXiv preprint arXiv:2308.15070*, 2023. 2
- [57] Guan-Hong Liu, Arash Vahdat, De-An Huang, Evangelos A Theodorou, Weili Nie, and Anima Anandkumar. I2sb: image-to-image schrödinger bridge. In *Proceedings of the 40th International Conference on Machine Learning*, pages 22042–22062, 2023. 2, 3
- [58] Jiawei Liu, Qiang Wang, Huijie Fan, Yinong Wang, Yandong Tang, and Liangqiong Qu. Residual denoising diffusion models. In *Proceedings of the IEEE/CVF Conference on Computer Vision and Pattern Recognition*, pages 2773–2783, 2024. 5
- [59] Qingguo Liu, Chenyi Zhuang, Pan Gao, and Jie Qin. Cdformer: When degradation prediction embraces diffusion model for blind image super-resolution. In *Proceedings of the IEEE/CVF Conference on Computer Vision and Pattern Recognition*, pages 7455–7464, 2024. 2
- [60] Andreas Lugmayr, Martin Danelljan, Andres Romero, Fisher Yu, Radu Timofte, and Luc Van Gool. Repaint: Inpainting using denoising diffusion probabilistic models. In *Proceedings of the IEEE/CVF Conference on Computer Vision and Pattern Recognition*, 2022. 2, 5
- [61] Youssef Mansour and Reinhard Heckel. Zero-shot noise2noise: Efficient image denoising without any data. In *Proceedings of the IEEE/CVF Conference on Computer Vision and Pattern Recognition*, pages 14018–14027, 2023. 2
- [62] Chenlin Meng, Yutong He, Yang Song, Jiaming Song, Jiajun Wu, Jun-Yan Zhu, and Stefano Ermon. Sdedit: Guided image synthesis and editing with stochastic differential equations. *arXiv preprint arXiv:2108.01073*, 2021. 2
- [63] Sachit Menon, Alexandru Damian, Shijia Hu, Nikhil Ravi, and Cynthia Rudin. Pulse: Self-supervised photo upsampling via latent space exploration of generative models. In *Proceedings of the IEEE/CVF Conference on Computer Vision and Pattern Recognition*, 2020. 2
- [64] Nick Moran, Dan Schmidt, Yu Zhong, and Patrick Coady. Noisier2noise: Learning to denoise from unpaired noisy data. In *Proceedings of the IEEE/CVF Conference on Computer Vision and Pattern Recognition*, pages 12064–12072, 2020. 2
- [65] Xingang Pan, Xiaohang Zhan, Bo Dai, Dahua Lin, Chen Change Loy, and Ping Luo. Exploiting deep generative prior for versatile image restoration and manipulation. In *European Conference on Computer Vision (ECCV)*, 2020. 2
- [66] Xingang Pan, Xiaohang Zhan, Bo Dai, Dahua Lin, Chen Change Loy, and Ping Luo. Exploiting deep generative prior for versatile image restoration and manipulation. *IEEE Transactions on Pattern Analysis and Machine Intelligence*, 2021.
- [67] Deepak Pathak, Philipp Krahenbuhl, Jeff Donahue, Trevor Darrell, and Alexei A Efros. Context encoders: Feature learning by inpainting. In *Proceedings of the IEEE/CVF Conference on Computer Vision and Pattern Recognition*, 2016. 2
- [68] Mengwei Ren, Mauricio Delbracio, Hossein Talebi, Guido Gerig, and Peyman Milanfar. Multiscale structure guided diffusion for image deblurring. In *Proceedings of the IEEE/CVF International Conference on Computer Vision*, pages 10721–10733, 2023. 2
- [69] William Hadley Richardson. Bayesian-based iterative method of image restoration. *JoSA*, 62(1):55–59, 1972. 2
- [70] Robin Rombach, Andreas Blattmann, Dominik Lorenz, Patrick Esser, and Björn Ommer. High-resolution image synthesis with latent diffusion models. In *Proceedings of the IEEE/CVF conference on computer vision and pattern recognition*, pages 10684–10695, 2022. 2
- [71] Robin Rombach, Andreas Blattmann, Dominik Lorenz, Patrick Esser, and Björn Ommer. High-resolution image synthesis with latent diffusion models. In *Proceedings of the IEEE/CVF Conference on Computer Vision and Pattern Recognition*, 2022. 2
- [72] Chitwan Saharia, William Chan, Huiwen Chang, Chris Lee, Jonathan Ho, Tim Salimans, David Fleet, and Mohammad Norouzi. Palette: Image-to-image diffusion models. In *ACM SIGGRAPH*, 2022. 2
- [73] Chitwan Saharia, Jonathan Ho, William Chan, Tim Salimans, David J Fleet, and Mohammad Norouzi. Image super-resolution via iterative refinement. *IEEE Transactions on Pattern Analysis and Machine Intelligence*, 2022. 2
- [74] Johannes Schwab, Stephan Antholzer, and Markus Haltmeier. Deep null space learning for inverse problems: convergence analysis and rates. *Inverse Problems*, 35(2), 2019. 3
- [75] Jascha Sohl-Dickstein, Eric Weiss, Niru Maheswaranathan, and Surya Ganguli. Deep unsupervised learning using nonequilibrium thermodynamics. In *International conference on machine learning*, pages 2256–2265. PMLR, 2015. 2
- [76] Jiaming Song, Chenlin Meng, and Stefano Ermon. Denoising diffusion implicit models. In *International conference on machine learning*, 2021. 2, 5
- [77] Jiaming Song, Arash Vahdat, Morteza Mardani, and Jan Kautz. Pseudoinverse-guided diffusion models for inverse problems. In *ICLR*, 2023. 3, 4, 5, 6
- [78] Yang Song and Stefano Ermon. Generative modeling by estimating gradients of the data distribution. *Advances in neural information processing systems*, 32, 2019. 2, 3
- [79] Yang Song, Jascha Sohl-Dickstein, Diederik P Kingma, Abhishek Kumar, Stefano Ermon, and Ben Poole. Score-based generative modeling through stochastic differential equations. In *International conference on machine learning*, 2021. 2, 3
- [80] Matthieu Terris, Thomas Moreau, Nelly Pustelnik, and Julian Tachella. Equivariant plug-and-play image reconstruction. In *Proceedings of the IEEE/CVF Conference on Computer Vision and Pattern Recognition*, pages 25255–25264, 2024. 2

- [81] Pascal Vincent. A connection between score matching and denoising autoencoders. *Neural computation*, 23(7):1661–1674, 2011. 3
- [82] Jiachuan Wang, Shimin Di, Lei Chen, and Charles Wang Wai Ng. Noise2info: Noisy image to information of noise for self-supervised image denoising. In *Proceedings of the IEEE/CVF International Conference on Computer Vision*, pages 16034–16043, 2023. 2
- [83] Jianyi Wang, Zongsheng Yue, Shangchen Zhou, Kelvin CK Chan, and Chen Change Loy. Exploiting diffusion prior for real-world image super-resolution. In *arXiv preprint arXiv:2305.07015*, 2023. 2
- [84] Xintao Wang, Ke Yu, Shixiang Wu, Jinjin Gu, Yihao Liu, Chao Dong, Yu Qiao, and Chen Change Loy. Esrgan: Enhanced super-resolution generative adversarial networks. In *ECCVW*, 2018. 2
- [85] Xintao Wang, Liangbin Xie, Chao Dong, and Ying Shan. Real-esrgan: Training real-world blind super-resolution with pure synthetic data. In *ICCVW*, 2021. 2
- [86] Yinhuai Wang, Yujie Hu, Jiwen Yu, and Jian Zhang. Gan prior based null-space learning for consistent super-resolution. In *Proceedings of the AAAI Conference on Artificial Intelligence*, pages 2724–2732, 2023. 3
- [87] Yinhuai Wang, Jiwen Yu, Runyi Yu, and Jian Zhang. Unlimited-size diffusion restoration. In *Proceedings of the IEEE/CVF Conference on Computer Vision and Pattern Recognition*, pages 1160–1167, 2023. 3
- [88] Yinhuai Wang, Jiwen Yu, and Jian Zhang. Zero-shot image restoration using denoising diffusion null-space model. In *International conference on machine learning*, 2023. 2, 3, 5, 6, 7, 8
- [89] Zhou Wang, Alan C Bovik, Hamid R Sheikh, and Eero P Simoncelli. Image quality assessment: from error visibility to structural similarity. *IEEE transactions on image processing*, 13(4):600–612, 2004. 6
- [90] Shuchen Weng, Peixuan Zhang, Yu Li, Si Li, Boxin Shi, et al. L-cad: Language-based colorization with any-level descriptions using diffusion priors. *Advances in Neural Information Processing Systems*, 36, 2024. 2
- [91] Jay Whang, Mauricio Delbracio, Hossein Talebi, Chitwan Saharia, Alexandros G Dimakis, and Peyman Milanfar. Deblurring via stochastic refinement. In *Proceedings of the IEEE/CVF Conference on Computer Vision and Pattern Recognition*, pages 16293–16303, 2022. 2
- [92] Jia-Hao Wu, Fu-Jen Tsai, Yan-Tsung Peng, Chung-Chi Tsai, Chia-Wen Lin, and Yen-Yu Lin. Id-blau: Image deblurring by implicit diffusion-based reblurring augmentation. In *Proceedings of the IEEE/CVF Conference on Computer Vision and Pattern Recognition*, pages 25847–25856, 2024. 2
- [93] Bin Xia, Yulun Zhang, Shiyin Wang, Yitong Wang, Xinglong Wu, Yapeng Tian, Wenming Yang, and Luc Van Gool. Diffir: Efficient diffusion model for image restoration. In *ICCV*, 2023. 2
- [94] Chaohao Xie, Shaohui Liu, Chao Li, Ming-Ming Cheng, Wangmeng Zuo, Xiao Liu, Shilei Wen, and Errui Ding. Image inpainting with learnable bidirectional attention maps. In *ICCV*, 2019. 2
- [95] Jun Xu, Yuan Huang, Ming-Ming Cheng, Li Liu, Fan Zhu, Zhou Xu, and Ling Shao. Noisy-as-clean: Learning self-supervised denoising from corrupted image. *IEEE Transactions on Image Processing*, 29:9316–9329, 2020. 2
- [96] Ruihan Yang and Stephan Mandt. Lossy image compression with conditional diffusion models. *Advances in Neural Information Processing Systems*, 36, 2024. 2
- [97] Tian Ye, Sixiang Chen, Wenhao Chai, Zhaohu Xing, Jing Qin, Ge Lin, and Lei Zhu. Learning diffusion texture priors for image restoration. In *Proceedings of the IEEE/CVF Conference on Computer Vision and Pattern Recognition*, pages 2524–2534, 2024. 2
- [98] Jiahui Yu, Zhe Lin, Jimei Yang, Xiaohui Shen, Xin Lu, and Thomas S Huang. Free-form image inpainting with gated convolution. In *ICCV*, 2019. 2
- [99] Zongsheng Yue and Chen Change Loy. Difface: Blind face restoration with diffused error contraction. *arXiv preprint arXiv:2212.06512*, 2022. 2
- [100] Syed Waqas Zamir, Aditya Arora, Salman Khan, Munawar Hayat, Fahad Shahbaz Khan, and Ming-Hsuan Yang. Restormer: Efficient transformer for high-resolution image restoration. In *Proceedings of the IEEE/CVF Conference on Computer Vision and Pattern Recognition*, 2022. 2
- [101] Yanhong Zeng, Jianlong Fu, Hongyang Chao, and Bain-ing Guo. Aggregated contextual transformations for high-resolution image inpainting. *TVCG*, 2022. 2
- [102] Kai Zhang, Yawei Li, Wangmeng Zuo, Lei Zhang, Luc Van Gool, and Radu Timofte. Plug-and-play image restoration with deep denoiser prior. *IEEE Transactions on Pattern Analysis and Machine Intelligence*, 2021. 2
- [103] Kai Zhang, Jingyun Liang, Luc Van Gool, and Radu Timofte. Designing a practical degradation model for deep blind image super-resolution. In *ICCV*, 2021. 2
- [104] Richard Zhang, Phillip Isola, Alexei A Efros, Eli Shechtman, and Oliver Wang. The unreasonable effectiveness of deep features as a perceptual metric. In *Proceedings of the IEEE conference on computer vision and pattern recognition*, pages 586–595, 2018. 6
- [105] Yuzhe Zhang, Jiawei Zhang, Hao Li, Zhouxia Wang, Luwei Hou, Dongqing Zou, and Liheng Bian. Diffusion-based blind text image super-resolution. In *Proceedings of the IEEE/CVF Conference on Computer Vision and Pattern Recognition*, pages 25827–25836, 2024. 2
- [106] Bo Zhou and S Kevin Zhou. Dudornet: learning a dual-domain recurrent network for fast mri reconstruction with deep t1 prior. In *Proceedings of the IEEE/CVF conference on computer vision and pattern recognition*, pages 4273–4282, 2020. 2
- [107] Yuanzhi Zhu, Kai Zhang, Jingyun Liang, Jie Zhang Cao, Bihan Wen, Radu Timofte, and Luc Van Gool. Denoising diffusion models for plug-and-play image restoration. In *Proceedings of the IEEE/CVF Conference on Computer Vision and Pattern RecognitionW*, 2023. 2